Reconstruction of Delayed Neutron Precursor Groups from Data

Luke Seifert[1], Benjamin Betzler[2], William Wieselquist[2], Matthew Jessee[2], Madicken Munk[1,3], Kathyrn Huff[1]

[1]*Advanced Reactors and Fuel Cycles Group, University of Illinois at Urbana-Champaign*
[2]*Nuclear Energy and Fuel Cycle Division, Oak Ridge National Laboratory, Oak Ridge, TN*
[3]*School of Nuclear Science and Engineering, Oregon State University, Corvallis, OR*

ABSTRACT

Delayed neutron precursor (DNP) groups are important for modeling reactor dynamics. Although the data on individual DNPs has been developed over time, the DNP group data present in the Evaluated Nuclear Data Files (ENDF) has not been updated in the past 20 years. This work uses SCALE to recreate the Godiva experiment that was used to generate the original fast fission of ^{235}U DNP group structure. However, each DNP is modeled using up-to-date data, and the results are then converted into a newly updated group structure. The conversion to group structure uses an iterative linear least squares solver to minimize chi-squared. This work also allows for energy spectra generation and uncertainty tracking. The method used in this paper for fast ^{235}U fission DNP group structure updating can be applied to different energies and fissile nuclides. This work allows for improved uncertainty tracking in reactor kinetics and dynamics, demonstrated through a point reactor kinetics simulation.

INTRODUCTION

Delayed neutron precursors (DNPs) are an important consideration in reactor operation and safety because the time delay before delayed neutrons are emitted allows for more precise control of nuclear reactors. The physical mechanism of DNPs is the process in which a beta-emitting isotope that has sufficient energy concurrently emits a neutron; thus, the neutron emission has the same half-life as the beta emission. Additionally, some isotopes have sufficient energy to emit multiple neutrons, each of which with different probabilities of occurring.

For many reactor applications, it is practical to divide the DNPs into six to eight groups per fissile isotope instead of modeling each DNP individually. Each of these groups has both a half-life and an abundance. The half-life of the group is based on the half-lives of the constituent DNPs in that group, while the abundance is based on the amount of DNPs in that group and the number of neutrons they emit. The differences in group half-lives and abundances between different isotopes are caused by the isotopic yield differences. These yield differences affect how the DNPs are generated, thus affecting the overall group structure.

Many updates to the available DNP data have been made, and many of these data have been collected in a database maintained by the International Atomic Energy Agency (IAEA) [1]. Although these more recent IAEA data exist, the DNP group data used in the Evaluated Nuclear Data File (ENDF)/B-VIII.0 library have not been updated since ENDF/B-VI.8 [2], approximately 20 years ago [3]. Additionally, the spectral data have not been updated in ~30 years [4, 5]. This work reconstructs the DNP groups using recent data to evaluate whether the groups must be altered.

METHODS

The DNP groups have historically been generated either experimentally or computationally by using the delayed neutron counts after irradiation [6, 7, 5, 8, 9]. In this work, the primary difference in the results come from the data used for the individual DNPs. For the DNP group spectral fits, there is a new method proposed in this work. This work also shows how the group fit results from different data compare when used in a point kinetics model. The uncertainties are tracked throughout, as the more recent individual DNP data has uncertainties which can be propagated.

The tools used in this work are in-house Python scripts and SCALE 6.3, within which TRITON and ORIGEN were used for most of the analysis. TRITON is a reactor physics and depletion sequence, and ORIGEN is a depletion and decay solver [10]. Specifically, the "T6-DEPL" TRITON sequence was used that enables TRITON to run with KENO-VI as neutron transport. POLARIS, which handles light water reactor lattice physics, was used for comparing the different DNP group fits after the results were generated.

The model of interest to start with is Godiva, a uniform sphere of ^{235}U with a diameter of $6\frac{3}{4}$ inches and density of 19 g/cm^3 [11]. The TRITON input deck was set to create Godiva and have a 0.25 ms pulse irradiation with roughly 10^{16} fission events. The Godiva sphere does not deplete, but rather a 3 gram sample within Godiva is irradiated, the same as in the Keepin, Wimett, and Zeigler experiment [6]. The irradiation was then followed by a 330 s decay of the sample using logarithmically spaced time nodes to capture the short-lived DNPs' response in ORIGEN. This method replicated the one used by Keepin, Wimett, and Zeigler so that the results could be directly compared [6]. In the Keepin, Wimett, and Zeigler experiment, the data of interest used for analysis is the delayed neutron count over time.

Using data from the Godiva simulation and recent experimental data that has been published, the delayed neutron count can be constructed. Equation (1) shows how the data comes

This manuscript has been authored by UT-Battelle, LLC under contract DE-AC05-00OR22725 with the US Department of Energy (DOE). The US government retains and the publisher, by accepting the article for publication, acknowledges that the US government retains a nonexclusive, paid-up, irrevocable, worldwide license to publish or reproduce the published form of this manuscript, or allow others to do so, for US government purposes. DOE will provide public access to these results of federally sponsored research in accordance with the DOE Public Access Plan (http://energy.gov/downloads/doe-public-access-plan).

* Corresponding author: Luke Seifert - seifert5@illinois.edu

together to form the delayed neutron count. This equation sums over all DNPs (the number of which can vary based on the dataset), and calculates the time dependent delayed neutron count from each. This contribution from each DNP is then multiplied by the efficiency of the neutron detector, ϵ. By adjusting the detector efficiency term in the equation, the delayed neutron count profile is set to align with the results from Keepin et al [6].

$$n_d(t) = \epsilon \sum_{i=1}^{DNPs} P_{n_i} \lambda_i N_i(t). \tag{1}$$

The concentrations of each DNP, $N_i(t)$, can be retrieved from the ORIGEN binary concentration file (output from ORIGEN, TRITON, and Polaris). These can then be combined with the emission probabilities, $P_{n,i}$, and decay constants, λ_i, for DNP i from the IAEA database to generate the neutron emission count as a function of time. This can then be combined with the detector efficiency term, ϵ, to generate the delayed neutron count.

In addition to computing $n_d(t)$ from ORIGEN concentrations and IAEA data for emission probabilities and decay constants, ORIGEN also provides $n_d(t)$ directly, using a modified ENDF/B-VII.0 dataset for emission probabilities and decay constants. More specifically, one approach uses SCALE 6.2.4 neutron emission, which uses an embedded version of SOURCES4C, combined with a modified ENDF/B-VII.0 dataset [12]. This approach is referred to as *Pure ORIGEN*, as it uses data taken purely from ORIGEN. The other approach uses ORIGEN concentrations and IAEA data for emission probabilities and decay constants, and it is referred to as *IAEA–ORIGEN*. For DNP data which is in ORIGEN but not the IAEA database, the IAEA-ORIGEN approach obtains data from the Evaluated Nuclear Structure Data File (ENSDF) and ENDF/B-VIII.1 to fill in gaps between the datasets [13, 2].

Group Fits

For a pulse irradiation with n groups and m time nodes, Equations (2)–(7) show how the iterative least squares problem is configured, where the λ_i values are determined by iterating through multiple possible values of each decay constant and checking each combination:

The general least squares problem being solved is given as

$$A\boldsymbol{x} \approx \boldsymbol{b}, \tag{2}$$

which can be rewritten more explicitly in the following form for a pulse irradiation:

$$n_d(t) \approx \epsilon F_s \sum_{i=1}^{n} a_i \lambda_i e^{-\lambda_i t}. \tag{3}$$

The a_i values are the group yield, or group abundance, values. These represent the number of delayed neutrons per fission; when summed, they provide the total delayed neutron yield per fission. The F_s value is the total number of fission events that take place within the sample, and ϵ is the detector efficiency. The efficiency of the neutron detector in this work, ϵ, is set so that the Keepin, Wimett, and Zeigler delayed neutron precursor count results, when using their group yields and decay constants, align with the reported counts [6]. The total number of delayed neutrons is known, as well as the number of fissions and efficiency term. The unknowns are the decay constants for each group, λ_i, and the group yields, a_i. However, by making guesses at the group decay constants, the problem can be formatted as follows:

$$\boldsymbol{x} = \begin{Vmatrix} a_1 \\ a_2 \\ \vdots \\ a_n \end{Vmatrix}, \tag{4}$$

$$A = \begin{Vmatrix} \lambda_1 e^{-\lambda_1 t_0} & \lambda_2 e^{-\lambda_2 t_0} & \dots & \lambda_n e^{-\lambda_n t_0} \\ \lambda_1 e^{-\lambda_1 t_1} & \lambda_2 e^{-\lambda_2 t_1} & \dots & \lambda_n e^{-\lambda_n t_1} \\ \vdots & \vdots & \ddots & \vdots \\ \lambda_1 e^{-\lambda_1 t_m} & \lambda_2 e^{-\lambda_2 t_m} & \dots & \lambda_n e^{-\lambda_n t_m} \end{Vmatrix}, \tag{5}$$

$$\boldsymbol{b} = \begin{Vmatrix} n_d(t_0)(\epsilon F_s)^{-1} \\ n_d(t_1)(\epsilon F_s)^{-1} \\ \vdots \\ n_d(t_m)(\epsilon F_s)^{-1} \end{Vmatrix}, \tag{6}$$

where the solution for the group yields with the guessed group decay constants is:

$$\boldsymbol{x} \approx (A^T A)^{-1} A^T \boldsymbol{b}. \tag{7}$$

An iterative process is used to improve the guess for the group decay constants such that the net delayed neutron emission curve is better modeled after each iteration. The iteration process goes through Equations (2)–(7) for various values of λ_i; then, the coarseness of the decay constant mesh is decreased, becoming finer until a more optimal solution is found based on minimizing the chi-squared measure, as shown in Equation (8). Once a new optimal solution is found, the process begins again with the most coarse mesh, where the λ_i values for a given group i are set to exist within a wide range which becomes smaller after each iteration. The iterations stop once a certain threshold is reached. In this work, the process was allowed to iterate until the point at which an adjustment of λ_i mesh values by 1% in either direction (i.e., 1% higher and lower) no longer improved the fit.

$$\chi^2 = \sum_{j=1}^{m} \left(\frac{y_j - \sum_{i=1}^{n} a_i \lambda_i e^{-\lambda_i t_j}}{\sigma_j} \right)^2, \tag{8}$$

where m is the total number of time nodes, n is the number of groups, y_j is the delayed neutron counts at time j, and σ_j is the uncertainty of those delayed neutron counts.

Spectral Fits

In the past, the spectral fits were generated by allowing each isotope to contribute some fraction to its closest groups, sorted by group half-life [14, 15, 5] or by sorting based on nuclide half-life [16, 17]. This work refers to such approaches as *fractional fitting least squares*. Alternatively, using an

iterative least squares technique allows for a more optimal set of group fits such that isotopes can contribute to more than two groups. This method also requires no individualized spectral data for the isotopes, yielding no potential error from erroneous spectral data within the fitting method. This method is referred to as *iterative least squares* in this work.

To determine the spectrum of each group, the delayed neutron emission rate as a function of time and energy, $n_d(E,t)$, can either be collected from the ORIGEN output or generated from the IAEA database using Equation (9):

$$n_d(E,t) = \epsilon \sum_{i=1}^{DNPs} \chi_i(E)\lambda_i N_i(t) P_{n_i}. \tag{9}$$

Once the two-dimensional set of values for $n_d(E,t)$ is collected, the group spectra are generated using iterative least squares. This method iterates through each possible energy bin while solving the least squares problem for every time node, thus optimizing every j^{th} energy bin for all times. Equations (10)–(13) show the iterative least squares method used, whereas Equations (14) and (15) show the solutions using ordinary least squares and using the percent regression least squares, respectively [18]:

$$n_d(E,t) \approx \epsilon F_s \sum_{i=1}^{n} \chi_i(E)\lambda_i a_i e^{-\lambda_i t}, \tag{10}$$

$$\boldsymbol{x} = \begin{Vmatrix} \chi_1(E_j) \\ \chi_2(E_j) \\ \vdots \\ \chi_n(E_j) \end{Vmatrix}, \tag{11}$$

$$A = \begin{Vmatrix} \lambda_1 a_1 e^{-\lambda_1 t_0} & \lambda_2 a_2 e^{-\lambda_2 t_0} & \dots & \lambda_n a_n e^{-\lambda_n t_0} \\ \lambda_1 a_1 e^{-\lambda_1 t_1} & \lambda_2 a_2 e^{-\lambda_2 t_1} & \dots & \lambda_n a_n e^{-\lambda_n t_1} \\ \vdots & \vdots & \ddots & \vdots \\ \lambda_1 a_1 e^{-\lambda_1 t_m} & \lambda_2 a_2 e^{-\lambda_2 t_m} & \dots & \lambda_n a_n e^{-\lambda_n t_m} \end{Vmatrix}, \tag{12}$$

$$\boldsymbol{b} = \begin{Vmatrix} n_d(E_j,t_0)(\epsilon F_s)^{-1} \\ n_d(E_j,t_1)(\epsilon F_s)^{-1} \\ \vdots \\ n_d(E_j,t_m)(\epsilon F_s)^{-1} \end{Vmatrix}, \tag{13}$$

$$\boldsymbol{x} \approx (A^T A)^{-1} A^T \boldsymbol{b}, \tag{14}$$

$$\boldsymbol{x} = (A^T D^2 A)^{-1} A^T D^2 \boldsymbol{b}. \tag{15}$$

In the formulations above, $\bar{\bar{D}}$ is a diagonal matrix containing the inverse of $\boldsymbol{b}$ along the diagonal. Equation (15) was incorporated into the non-negative least squares method in the outer loop, whereas the residual in the outer loop was adjusted to solve the residual equation shown in Equation (16) [19]:

$$argmin_x \left\| \frac{Ax-b}{b} \right\|_2. \tag{16}$$

This approach's main issues consist of its computational cost, the occasional negative probability calculated for a group spectrum, and the possibility of a poor fit at later times. Although the computational cost issue will remain, the other issues can be solved by implementing a combination of non-negative least squares and least squares percentage regression techniques [19, 18]. However, it was found that a more optimal solution is generated by instead implementing the least squares percentage regression and then setting any negative values to 0.

Point Reactor Kinetics

Using the point reactor kinetics equations enables an understanding of how the group fits will affect the system on a more macroscopic scale. Equation (17) provides the initial conditions used, whereas Equations (18) and (19) are the general forms of the neutron density and precursor concentrations equations, respectively:

$$\begin{cases} n_0 = 1 \\ c_{i_0} = \beta_i n_0 (\lambda_i \Lambda)^{-1} \end{cases}, \tag{17}$$

$$\frac{dn}{dt} = \frac{\rho - \beta}{\Lambda} n(t) + \sum_{i=1}^{6} \lambda_i C_i(t), \tag{18}$$

$$\frac{dC_i}{dt} = \frac{\beta_i}{\Lambda} n(t) - \lambda_i C_i(t). \tag{19}$$

The Λ term is the neutron generation time, ρ is the reactivity, and the β_i values are calculated using the group yields and average neutron emission per fission event, as shown in Equation (35):

$$\beta_i = \frac{a_i}{\bar{\nu}}. \tag{20}$$

In this work, the equations were solved iteratively, and each subsequent term was calculated using the forward Euler method, shown in Equations (21) and (22):

$$n_{cur} = n_{prev} + \frac{dn_{prev}}{dt}\Delta t, \tag{21}$$

$$C_{i_{cur}} = C_{i_{prev}} + \frac{dC_{i_{prev}}}{dt}\Delta t. \tag{22}$$

The forward Euler method is not an optimal approach to generating results for the point reactor kinetics equations; however, generating and providing sufficiently accurate results that demonstrated the differences yielded from each data set is simple using this approach.

Uncertainties

Important considerations for these methods are the uncertainties in the data used and how the data change based on the method used. For the group fit uncertainty, previous work by the authors showed that the data include decay constants, delayed neutron emission counts, and fissions [20].

For the group fit construction uncertainty, the uncertainty in the delayed neutron emission counts from ORIGEN can be determined based on Equation (9) by using Equations (23)–(26). This uncertainty is then used in Equations (27)–(30) to calculate the uncertainty for the entire right-hand side.

The uncertainty in the emission probabilities, ΔP_{n_i}, comes from the IAEA data; the uncertainty in concentration, ΔN_{0_i}, comes from Sampler in SCALE [10]; and the uncertainty in the decay constants, $\Delta\lambda_i$, comes from the IAEA data for the ORIGEN delayed neutron counts and is based on the mesh for the group fit. Sampler is used with 500 samples, with perturbations in each non-metastable nuclide of cross sections, yields, and decay constants.

From Equation (9), partial derivatives are taken, yielding Equations (23)–(25). These partial derivatives are then used in the uncertainty calculation in the delayed neutron count from each individual delayed neutron precursor as shown in Equation (26).

$$\frac{\partial n_d(t)}{\partial P_{n_i}} = \lambda_i N_{0_i} e^{-\lambda_i t}, \tag{23}$$

$$\frac{\partial n_d(t)}{\partial \lambda_i} = P_{n_i} N_{0_i} (1 - \lambda_i t) e^{-\lambda_i t}, \tag{24}$$

$$\frac{\partial n_d(t)}{\partial N_{0_i}} = P_{n_i} \lambda_i e^{-\lambda_i t}, \tag{25}$$

$$\Delta n_d^2(t) = \epsilon \sum_{i=1}^{n} \left(\frac{\partial n_d(t)}{\partial P_{n_i}} \Delta P_{n_i} \right)^2 + \left(\frac{\partial n_d(t)}{\partial \lambda_i} \Delta \lambda_i \right)^2 + \left(\frac{\partial n_d(t)}{\partial N_{0_i}} \Delta N_{0_i} \right)^2. \tag{26}$$

Equation (27) is the right-hand side vector at a point in time m used when solving for group fits. Partial derivatives are taken, shown in Equations (28) and (29). These partial derivatives are then used to generate the uncertainty at that time, shown in Equation (30).

$$\boldsymbol{b}_m = \frac{n_d(t_m)}{\epsilon F_s}. \tag{27}$$

$$\frac{\partial \boldsymbol{b}_m}{\partial n_d(t_m)} = \frac{1}{\epsilon F_s}, \tag{28}$$

$$\frac{\partial \boldsymbol{b}_m}{\partial F_s} = -\frac{n_d(t_m)}{\epsilon F_s^2}, \tag{29}$$

$$\Delta \boldsymbol{b}_m = \frac{1}{\epsilon} \sqrt{\left(\frac{\partial \boldsymbol{b}_m}{\partial n_d(t_m)} \Delta n_d(t_m) \right)^2 + \left(\frac{\partial \boldsymbol{b}_m}{\partial F_s} \Delta F_s \right)^2}. \tag{30}$$

The uncertainty in the group fit delayed neutron emission counts can be found using Equations (3) and the partial derivatives in Equations (31)–(32), yielding the result in Equation (33).

$$\frac{\partial n_d}{\partial a_i} = \lambda_i e^{-\lambda_i t}, \tag{31}$$

$$\frac{\partial n_d}{\partial \lambda_i} = a_i (1 - \lambda_i t) e^{-\lambda_i t}, \tag{32}$$

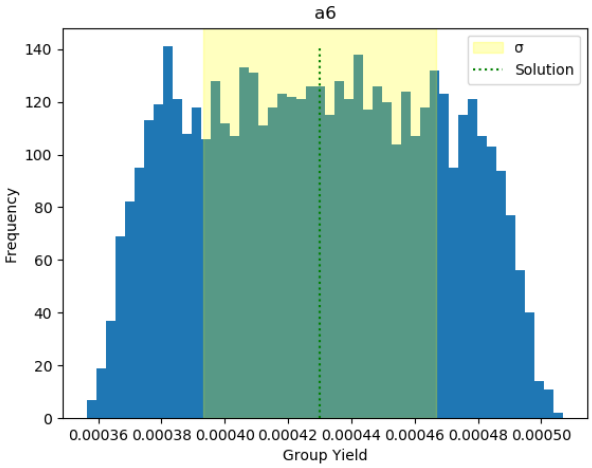

Fig. 1: Keepin, Wimett, and Zeigler six group data fitting at a 0.5% meshing of half-lives from a start of 5% with three possible half-lives per group and using 5,000 stochastic uncertainty runs.

$$\Delta n_d(t) = \epsilon F_s \sqrt{\sum_{i=1}^{n} \left(\frac{\partial n_d}{\partial a_i} \Delta a_i \right)^2 + \left(\frac{\partial n_d}{\partial \lambda_i} \Delta \lambda_i \right)^2}. \tag{33}$$

The uncertainty in the group yield values, Δa_i, was calculated using a stochastic approach. The least squares problem used to solve for a_i was iterated upon with random variations within uncertainties for the different terms until the point at which a normal distribution formed and the standard deviation could be directly extracted. An example of this approach is shown Figure 1, in which the sixth group yield is $(4.3 \pm 0.4) \times 10^{-4}$ delayed neutrons per fission.

Following the group fit are the point reactor kinetics uncertainties that use forward Euler. The decay constant uncertainty comes from the group fits; the initial uncertainties in both the number of neutrons at the current time, Δn_{cur}, and the number of precursors in the i^{th} group, $\Delta C_{i,cur}$, are zero; and the group and total delayed neutron fraction uncertainties, $\Delta\beta_i$ and $\Delta\beta$, respectively, are given in Equations (34) and (35):

$$\Delta\beta_i = \sqrt{\left(\frac{1}{\bar{\nu}} \Delta a_i \right)^2 + \left(\frac{a_i}{\bar{\nu}^2} \Delta \bar{\nu} \right)^2}, \tag{34}$$

$$\Delta\beta = \sqrt{\left(\sum_{i=1}^{n} \Delta\beta_i^2 \right)}. \tag{35}$$

The uncertainty in n_{cur} from Equation (21), rewritten explicitly in Equation (36), is given in Equation (42), with the components given in Equations (37)–(41). In these equations, Δt is the time step used in forward Euler:

$$n_{cur} = n_{prev} + \frac{\rho - \beta}{\Lambda} n_{prev} \Delta t + \sum_{i=1}^{n} \left(\lambda_i C_{i,prev} \Delta t + \frac{\beta_i}{\Lambda} n_{prev} \lambda_i \Delta t^2 - \lambda_i^2 C_{i,prev} \Delta t^2 \right), \quad (36)$$

$$\frac{\partial n_{cur}}{\partial n_{prev}} = 1 + \frac{\rho - \beta}{\Lambda} \Delta t + \sum_{i=1}^{n} \frac{\beta_i}{\Lambda} \lambda_i \Delta t^2, \quad (37)$$

$$\frac{\partial n_{cur}}{\partial \lambda_i} = C_{i,prev} \Delta t + \frac{\beta_i}{\Lambda} n_{prev} \Delta t^2 - 2\lambda_i C_{i,prev} \Delta t^2, \quad (38)$$

$$\frac{\partial n_{cur}}{\partial \beta} = \frac{-n_{prev} \Delta t}{\Lambda}, \quad (39)$$

$$\frac{\partial n_{cur}}{\partial \beta_i} = \frac{n_{prev} \lambda_i \Delta t^2}{\Lambda}, \quad (40)$$

$$\frac{\partial n_{cur}}{\partial C_{i,prev}} = \lambda_i \Delta t - \lambda_i^2 \Delta t^2, \quad (41)$$

$$\Delta n_{cur}^2 = \sum_{i=1}^{n} \left(\frac{\partial n(t)}{\partial n_{prev}} \Delta n_{prev} \right)^2 + \left(\frac{\partial n(t)}{\partial \lambda_i} \Delta \lambda_i \right)^2 + \left(\frac{\partial n(t)}{\partial \beta} \Delta \beta \right)^2 + \left(\frac{\partial n(t)}{\partial \beta_i} \Delta \beta_i \right)^2 + \left(\frac{\partial n(t)}{\partial C_{i,prev}} \Delta C_{i,prev} \right)^2. \quad (42)$$

The uncertainty in C_i from (22), rewritten explicitly in Equation (43), is given by Equation (48), incorporating the components given by Equations (44)–(47):

$$C_{i,cur} = C_{i,prev} + \frac{\beta_i}{\Lambda} n_{prev} \Delta t - \lambda_i \Delta t C_{i,prev}, \quad (43)$$

$$\frac{\partial C_i(t)}{\partial C_{i,prev}} = 1 - \lambda_i \Delta t, \quad (44)$$

$$\frac{\partial C_i(t)}{\partial \beta_i} = \frac{n_{prev} \Delta t}{\Lambda}, \quad (45)$$

$$\frac{\partial C_i(t)}{\partial n_{prev}} = \frac{\beta_i \Delta t}{\Lambda}, \quad (46)$$

$$\frac{\partial C_i(t)}{\partial \lambda_i} = -C_{i,prev} \Delta t, \quad (47)$$

$$\Delta C_i^2 = \sum_{i=1}^{n} \left(\frac{\partial C_i(t)}{\partial n_{prev}} \Delta n_{prev} \right)^2 + \left(\frac{\partial C_i(t)}{\partial \lambda_i} \Delta \lambda_i \right)^2 + \left(\frac{\partial C_i(t)}{\partial \beta_i} \Delta \beta_i \right)^2 + \left(\frac{\partial C_i(t)}{\partial C_{i,prev}} \Delta C_{i,prev} \right)^2. \quad (48)$$

Finally, for the group spectra constructed using the iterative linear least squares procedure, the uncertainty that is sought is shown in Equation (49). This uncertainty is fairly straightforward to calculate because the delayed neutron count term, $n_d(t)$, comes from the six group fit, and the uncertainty has already been discussed. The uncertainty for the energy-dependent neutron emission counts is shown in Equation (50), where the uncertainty in the spectra, $\Delta\chi_i(E)$, is calculated in the same manner as the uncertainty in the group yield values:

$$n_d(E,t) = n_d(t) \sum_i \chi_i(E), \quad (49)$$

$$\Delta n_d^2(E,t) = \left(\Delta n_d(t) \sum_i \chi_i(E) \right)^2 + (n_d(t))^2 \sum_i (\Delta \chi_i(E))^2. \quad (50)$$

RESULTS AND ANALYSIS

ORIGEN Data Compared with IAEA Data

Because the group fits will be made to fit the delayed neutron count data, it is important to understand how the data compare. The two different datasets compared are the IAEA database and the "end7dec" default decay ORIGEN library—referred to as *Pure ORIGEN*, *Pure*, or simply *ORIGEN*—which uses modified ENDF/B-VII.0 data and an embedded version of SOURCES4C. For analysis of delayed neutron emission counts, the three components that can change because of data are the time-dependent compositions, the decay constants, and the emission probabilities, all of which can be seen in Equation (1).

The composition as a function of time depends on the incident fission neutron energy, the fission yield, the decay constant of the target isotope, and that same data for any isotopes that decay into the target isotope. In this work, the ORIGEN- and IAEA-based data comparisons use the compositions generated by KENO-VI and decayed in ORIGEN.

The decay constants and emission probabilities, or branching fractions, can be tested by comparing the results of the Pure ORIGEN dataset simulated in ORIGEN with the IAEA dataset in ORIGEN. Specifically, we can adjust the data such that only decay constants, only emission probabilities, or both are changed from the Pure ORIGEN dataset values to the IAEA dataset values.

Figure 2 shows the net counts for the Pure ORIGEN and for the IAEA–ORIGEN data sets in which the percent difference appears to be close. The percent difference between the count rates was small at first, peaked at a 14% difference, and then dropped again. From the shape of the percent difference, it appears that short-lived isotopes decay away and reduce the difference.

Figures 3–5 provide more information on the short-lived and longer-lived isotopes that caused the discrepancy between the different sets of data. Figure 3 shows that the peak decay constant difference causes around 1.2 million counts per second, while the difference drops rapidly during later times. The emission probabilities have a smaller maximum effect, but the integral effect is larger; therefore, the combined effects of emission and decay constants are dominated by precursors

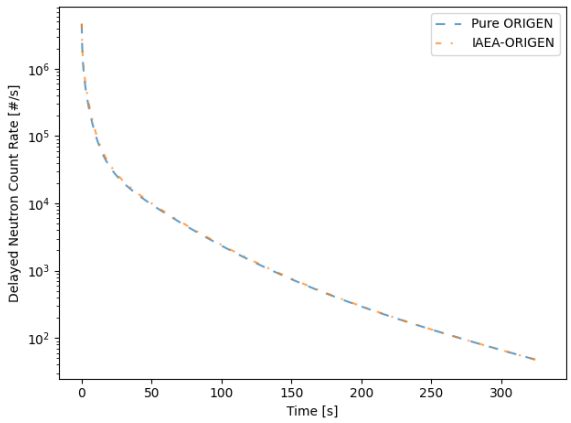

(a) Pure ORIGEN and IAEA ORIGEN count rate over time

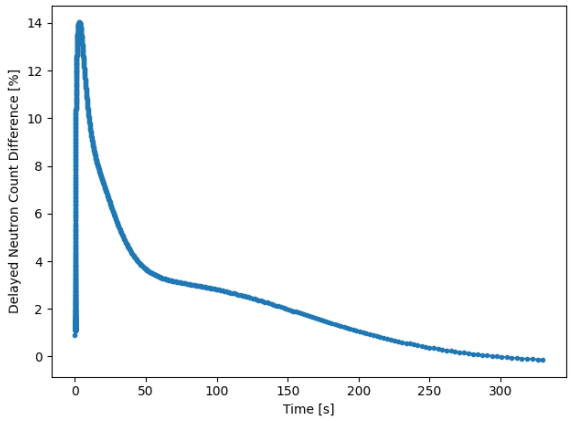

(b) Pure ORIGEN and IAEA ORIGEN count rate difference over time

Fig. 2: Comparison of delayed neutron count rate for Pure ORIGEN and IAEA ORIGEN data after fast-pulse irradiation of ^{235}U.

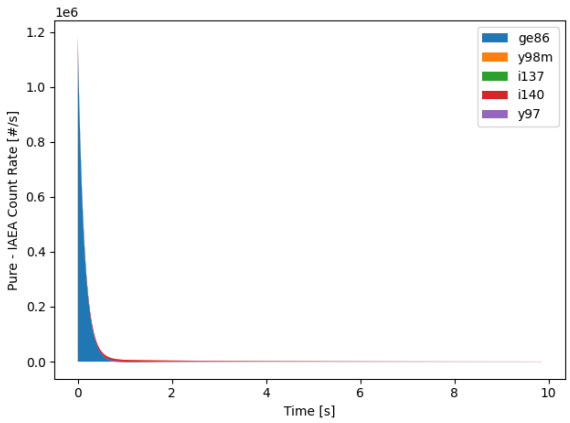

(a) Short time scale

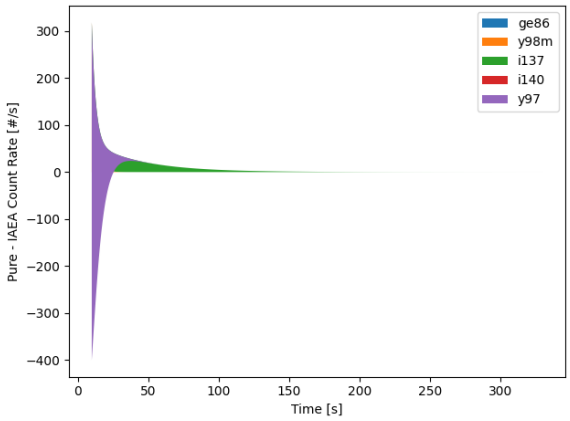

(b) Long time scale

Fig. 3: Decay constant–based difference between count rates with IAEA decay constants for ^{235}U fast-pulse irradiation over different time frames.

that are significantly affected by emission probability data differences.

Table I lists the isotopes that have the most significant effect on the decay constant and emission probability data differences. Figures 4 and 5 show the impact these nuclides have on the delayed neutron count rate. Based on Table I, it can be seen that the main difference in the delayed neutron count rates is caused by emission probabilities. This is because the predominant net difference is a result of the emission probability, which is further shown in Table II, where changing the decay data source only slightly affects the total delayed neutron yield while changing the emission probability data source changes the yield by approximately 200 pcm.

Figure 6 shows how the initial spectra of the ORIGEN output vary from the IAEA–ORIGEN spectra. Although these results account for only one time step, the spectral differences become smaller over time, as shown in Figure 7. This discrepancy at short time steps aligns with the previously discussed results. Additionally, because the main differences occur in the first 2 s, the problematic isotopes can be determined directly. The results shown in Figures 3–5 indicate that those isotopes that differ most significantly within the first 2 s are ^{91}Br, ^{85}As, ^{86}As, ^{137}I, and ^{138}I.

Six Group Fits

The DNP six groups can be calculated using the generated delayed neutron count rate data and iterative least squares method. An efficiency term of 3.75E-8 was used to align the Keepin group fit with the data presented in the Keepin, Wimett, and Zeigler paper [6]. This efficiency term was also used for the other results so that they could all be compared directly.

Table II lists the net yield variance observed between the IAEA data and ORIGEN library data. Additionally, net yields from other works are shown for fast ^{235}U irradiation.

Emission probability is the principal reason yield varied between the IAEA data and the ORIGEN decay library; a shift in the decay constant data minimally affects the net yield. Additionally, the net yields range from 0.0165 to 0.206 in the literature, which is a fairly large range of values. The current

TABLE I: Difference in data for isotopes with the largest difference in counts.

Isotope	λ_{IAEA}	λ_{ORIGEN}	P_{IAEA}	P_{ORIGEN}
^{91}Br	1.27	1.28	0.304	0.109
^{85}As	0.343	0.343	0.625	0.22
^{86}As	0.734	0.733	0.345	0.105
^{137}I	0.028	0.028	0.076	0.072
^{138}I	0.111	0.111	0.053	0.026
^{86}Ge	3.12	7.30	0.45	0.22
^{98m}Y	0.299	0.347	0.034	0.034
^{140}I	1.17	0.806	0.079	0.22
^{97}Y	0.185	0.185	5.8E-4	0.003

TABLE II: Net yields from various sources of data (partially recreated from [15]).

λ	P_n	Yield
IAEA	IAEA	0.0191
ORIGEN	IAEA	0.0193
IAEA	ORIGEN	0.0172
ORIGEN	ORIGEN	0.0172
Keepin et al. [6]	Keepin et al. [6]	0.0165
Brady/England [15]	Brady/England [15]	0.0206
Tuttle [21]	Tuttle [21]	0.0167
ENDF/B-V [22]	ENDF/B-V [22]	0.0167
England et al. [23]	England et al. [23]	0.0198
England/Rider [24]	England/Rider [24]	0.0206

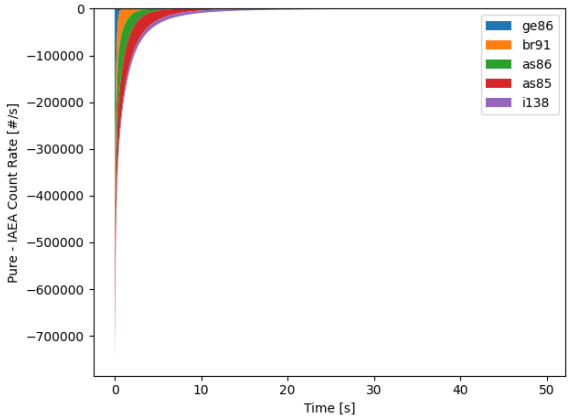

(a) Short time scale

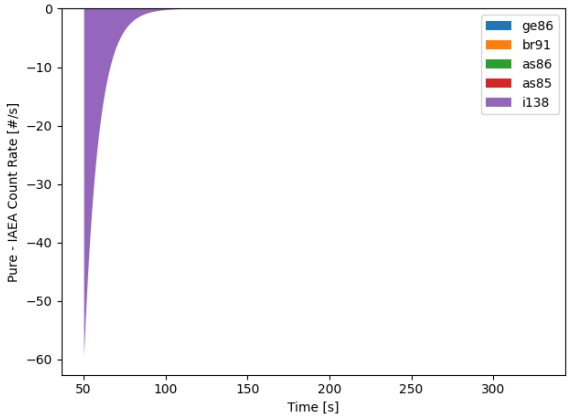

(b) Long time scale

Fig. 4: Emission probability (i.e., branching fraction)–based difference between count rates with IAEA decay constants for ^{235}U fast-pulse irradiation over different time frames.

TABLE III: Six group fit half-life parameters given in seconds.

Fit	T_1	T_2	T_3	T_4	T_5	T_6
[15]	52.1	21.2	5.74	2.29	0.816	0.243
[6]	54.5	21.8	6.00	2.23	0.496	0.179
IAEA	49.0	19.2	3.64	1.28	0.320	0.098
Pure	51.3	20.7	6.04	2.19	0.505	0.115

work's values fall within this range.

Tables III and V contain the group fit parameters, which were identified using the iterative least squares approach and the group fit parameters taken from Brady and England and from Keepin, Wimett, and Zeigler [15, 6]. The uncertainties for the group fits are given in Tables IV and VI.

In the group half-life fitting performed by the IAEA, each group exhibited a shorter half-life compared with all other fits. For the group yields, the IAEA fit showed greater weight on the longer-lived groups, which is noticeable when comparing the longest- and shortest-lived group yields. A comparison of the fits is shown in Figure 8; this comparison indicates

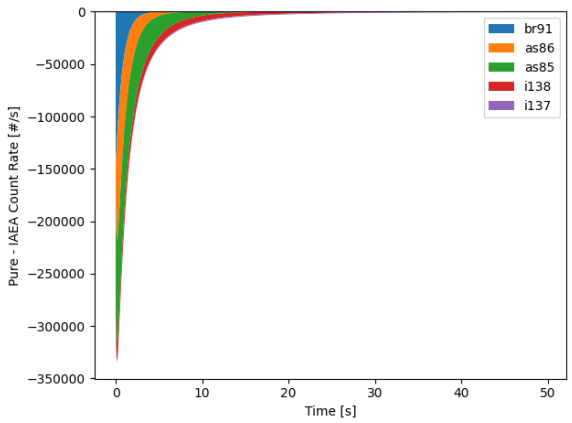

(a) Short time scale

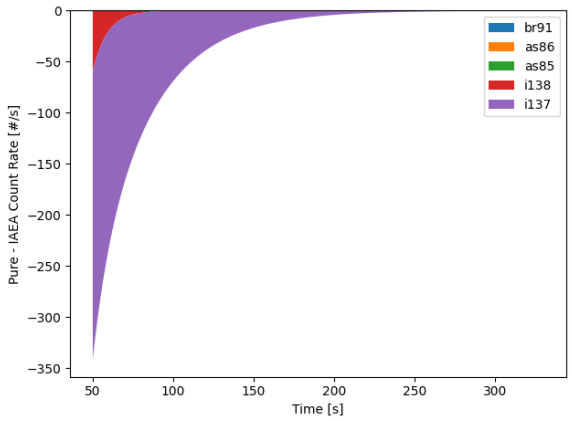

(b) Long time scale

Fig. 5: Combined decay constant and emission probability–based difference between count rates with IAEA decay constants for ^{235}U fast-pulse irradiation over different time frames.

TABLE IV: Six group fit half-life parameters' uncertainties given in seconds.

Fit	ΔT_1	ΔT_2	ΔT_3	ΔT_4	ΔT_5	ΔT_6
[6]	0.94	0.54	0.17	0.06	0.03	0.02
IAEA	0.245	0.096	0.018	0.006	0.002	0.001
Pure	0.256	0.104	0.030	0.011	0.003	0.001

that the current work's group fits are similar to other methods. The comparison also reveals discrepancies among the other referenced fits, although all of the fits shown are for the same fissile isotope and fast energy spectrum.

The discrepancies could be the result of differences in energy spectra causing fission, uncertainty in the number of fission events, uncertainty in the experimental data collected by Keepin, Wimett, and Zeigler (which were fitted), and uncertainty in the nuclear data used in the codes in this work and in Brady and England's work.

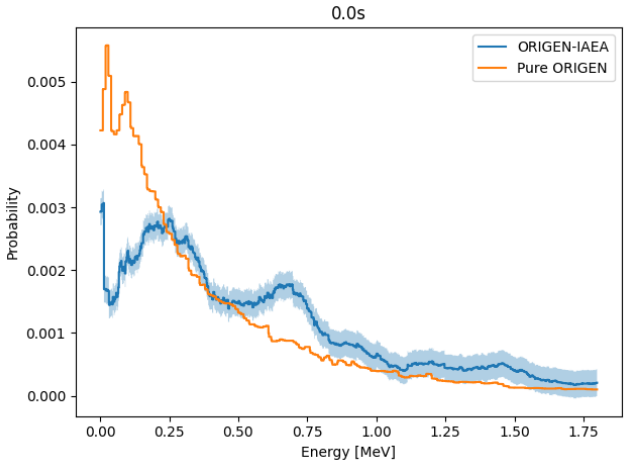

Fig. 6: Normalized difference in emission spectra of Pure ORIGEN and IAEA–ORIGEN for ^{235}U fast-pulse irradiation at 0 s.

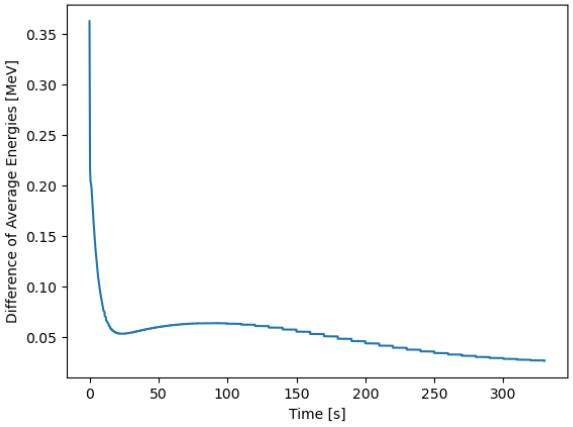

Fig. 7: Difference in average neutron energy from Pure ORIGEN and IAEA–ORIGEN for ^{235}U fast-pulse irradiation over time.

TABLE V: Six group fit yield parameters in delayed neutrons per fission multiplied by 100.

Fit	a_1	a_2	a_3	a_4	a_5	a_6
[15]	0.072	0.372	0.355	0.797	0.327	0.137
[6]	0.063	0.351	0.310	0.672	0.211	0.043
IAEA	0.083	0.350	0.670	0.566	0.187	0.054
Pure	0.071	0.308	0.244	0.711	0.300	0.091

TABLE VI: Six group fit yield parameters' uncertainties in delayed neutrons per fission multiplied by 100.

Fit	Δa_1	Δa_2	Δa_3	Δa_4	Δa_5	Δa_6
Keepin	0.005	0.011	0.028	0.023	0.015	0.005
IAEA	0.009	0.009	0.008	0.003	0.003	0.001
Pure	0.014	0.018	0.012	0.007	0.002	0.001

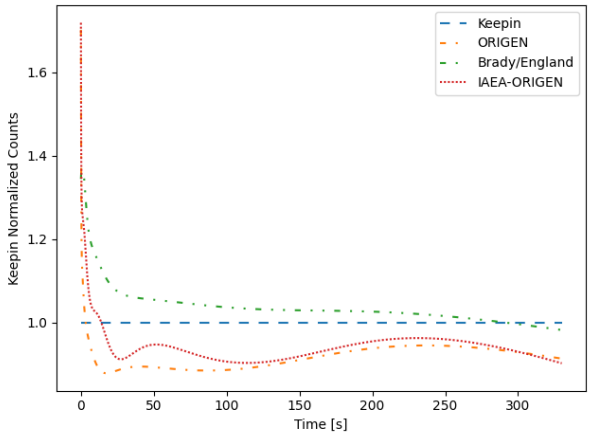

Fig. 8: A comparison of the different fast fission irradiation DNP six group fits of ^{235}U normalized to the Keepin, Wimett, and Zeigler six group fit count rate [6].

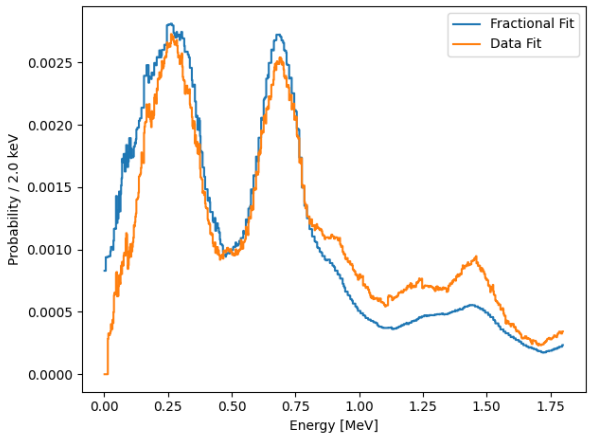

Fig. 9: Comparison of fractional fitting least squares method and iterative least squares method for the sixth precursor group for IAEA-ORIGEN in ^{235}U fast-pulse irradiation.

Six Group Spectra

Using the six group fits generated, as well as the energy-dependent count rate from ORIGEN and the constructed data from the IAEA database, the spectral profiles associated with each group can be generated, as shown in Equation (10). Figure 9 shows a comparison of the fractional fitting method and the iterative least squares method, labeled as "Data Fit", implemented in this work.

Figure 10 further compares the discrepancy between the historical fractional fitting approach and the proposed iterative least squares approach. The iterative least squares provided a much better fit than that of the fractional fitting method. This is shown at 330 s, but it is valid across the other times as well.

Point Reactor Kinetics Reactivity Insertion

To produce a macroscopic view of the effect of altering the group fit, the response to a reactivity step insertion can

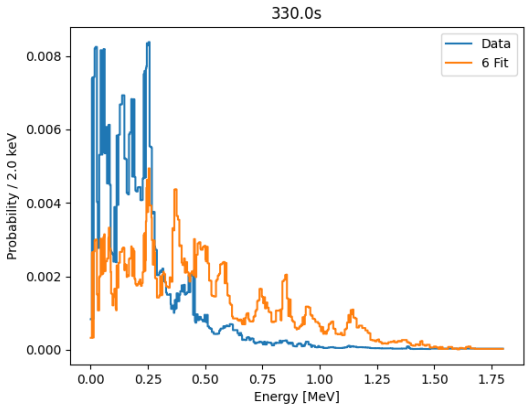

(a) Fractional fitting

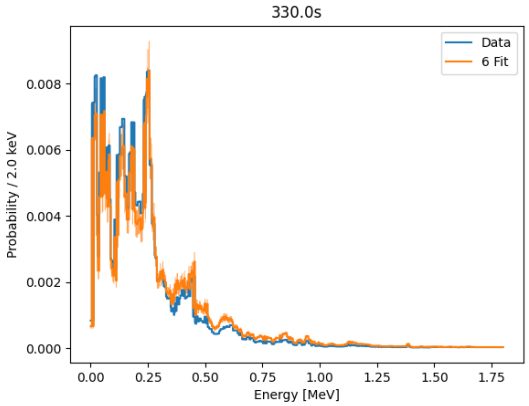

(b) Iterative least squares

Fig. 10: Comparison of data with normalized IAEA-ORIGEN six group spectra for ^{235}U pulse irradiation at 330 seconds.

be modeled using point reactor kinetics. Figure 11 shows the neutron density response to a reactivity step insertion into a reactor with a neutron generation time of 0.1 μs and average number of total neutrons per fission of 2.6.

Figure 11 shows that the Keepin, Wimett, and Zeigler response was slightly lower than that of the current work [6]. The responses began closely aligned and diverged further apart as the effect of the DNPs becomes more significant. In the later times, the IAEA–ORIGEN neutron density was slightly lower than the Pure ORIGEN neutron density. This is because the group fit of Pure ORIGEN has higher yield values for five and six groups, the yield values of which dominate during the early times. This effect was counteracted slightly by the slightly longer lives of five and six groups that Pure ORIGEN also has, but the net effect was still an increased response compared with that of the IAEA–ORIGEN group fit. Following this logic, the Keepin, Wimett, and Zeigler group fit has small yields for five and six groups while also having fairly long half- lives for each group.

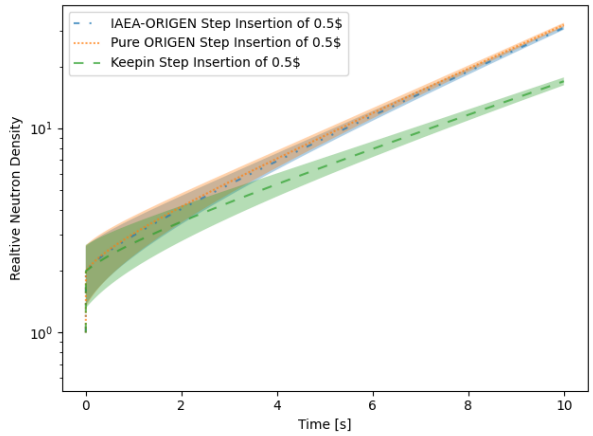

Fig. 11: Point reactor kinetic neutron density response to reactivity step insertion for different six group fits.

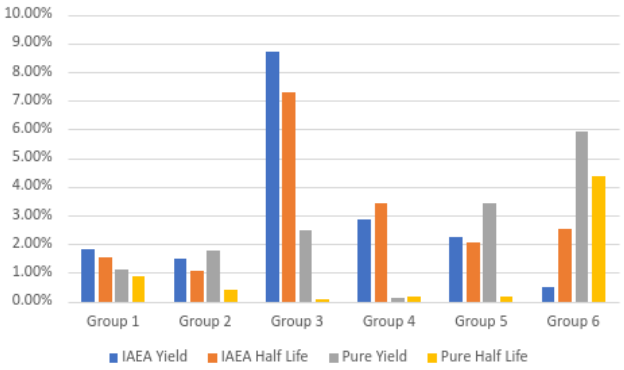

Fig. 12: The absolute percent difference of IAEA and Pure ORIGEN six group fits to the Keepin, Wimett, and Zeigler fits of fast spectrum U^{235} in a Westinghouse 17×17 fuel assembly.

Westinghouse 17×17 Pressurized Water Reactor

Additional macroscopic analysis was conducted using SCALE/Polaris. SCALE/Polaris is a tool used to perform 2D lattice physics that provides six group kinetics parameters as an output. These outputs are importance weighted, nuclide integrated, and assembly homogenized. Because these kinetics parameters are used by other codes to perform transient analyses, it is important to determine the difference using the default kinetic parameters used as an input compared with the six group fits generated in this work.

For this analysis, only the fast-spectrum kinetics parameters were altered for ^{235}U. This adjustmented was performed to provide a conservative estimate for the magnitude of difference, which can be expected because of the heavily thermal spectrum.

The default values used for the kinetic parameter inputs are those from Keepin, Wimett, and Zeigler [6]. The IAEA and Pure ORIGEN six group fits presented in this work were then used. The resulting kinetics parameters outputs for each set of group fits were compared with the absolute percent differences shown in Figure 12.

These absolute percent differences from the Keepin, Wimett, and Zeigler data show that the largest difference in IAEA yield and half-life values was observed in the third precursor group; the greatest difference in those values for Pure ORIGEN was observed in the sixth precursor group. This result corresponds directly to the differences in the six group fits shown in Tables III and V.

CONCLUSIONS AND FUTURE WORK

This work shows that the updated DNP data from the IAEA database differ from previous data; in particular, a few key isotopes have a large effect on these results because of differences in their data. Discrepancies among the data between SOURCES4C and the ENDF are currently being dealt with by relying more on ENDF and less on SOURCES4C where possible in SCALE. Additionally, corresponding updates could be made to the group fits by implementing updated data and propagating uncertainty. These updated DNP groups also suggest updates to the DNP group spectra, which could include uncertainty propagation and analysis of different methods to fit optimal spectra.

Further work to consider is a thorough analysis of different group fitting methods for yields, abundances, and spectra. This could include using non-linear least squares or other least squares methods, calculating uncertainty when the decay constant mesh is refined to the furthest extent possible, and determining whether other methods would alter how many groups are needed for a fit within a given margin. Additional work includes analysis of other data files, such as those of the Joint Evaluated Fission and Fusion library , to identify the presence of any isotopes causing discrepancies when compared with more recent data.

ACKNOWLEDGMENTS

This material is based upon work supported under an Integrated University Program Graduate Fellowship. The authors are grateful for this generous support. Thanks to Friederike Bostelmann and Ugur Mertyurek for their review of this paper.

REFERENCES

1. P. DIMITRIOU, I. DILLMANN, B. SINGH, V. PIKSAIKIN, K. RYKACZEWSKI, J. TAIN, A. ALGORA, K. BANERJEE, I. BORZOV, D. CANO-OTT, S. CHIBA, M. FALLOT, D. FOLIGNO, R. GRZYWACZ, X. HUANG, T. MARKETIN, F. MINATO, G. MUKHERJEE, B. RASCO, A. SONZOGNI, M. VERPELLI, A. EGOROV, M. ESTIENNE, L. GIOT, D. GREMYACHKIN, M. MADURGA, E. MCCUTCHAN, E. MENDOZA, K. MITROFANOV, M. NARBONNE, P. ROMOJARO, A. SANCHEZ-CABALLERO, and N. SCIELZO, "Development of a Reference Database for Beta-Delayed Neutron Emission," Nuclear Data Sheets, **173**, 144–238 (2021), special Issue on Nuclear Reaction Data.
2. D. BROWN, M. CHADWICK, R. CAPOTE, A. KAHLER, A. TRKOV, M. HERMAN, A. SONZOGNI, Y. DANON, A. CARLSON, M. DUNN, D. SMITH, G. HALE, G. ARBANAS, R. ARCILLA,

C. BATES, B. BECK, B. BECKER, F. BROWN, R. CASPERSON, J. CONLIN, D. CULLEN, M.-A. DESCALLE, R. FIRESTONE, T. GAINES, K. GUBER, A. HAWARI, J. HOLMES, T. JOHNSON, T. KAWANO, B. KIEDROWSKI, A. KONING, S. KOPECKY, L. LEAL, J. LESTONE, C. LUBITZ, J. MÁRQUEZ DAMIÁN, C. MATTOON, E. MCCUTCHAN, S. MUGHABGHAB, P. NAVRATIL, D. NEUDECKER, G. NOBRE, G. NOGUERE, M. PARIS, M. PIGNI, A. PLOMPEN, B. PRITYCHENKO, V. PRONYAEV, D. ROUBTSOV, D. ROCHMAN, P. ROMANO, P. SCHILLEBEECKX, S. SIMAKOV, M. SIN, I. SIRAKOV, B. SLEAFORD, V. SOBES, E. SOUKHOVITSKII, I. STETCU, P. TALOU, I. THOMPSON, S. VAN DER MARCK, L. WELSER-SHERRILL, D. WIARDA, M. WHITE, J. WORMALD, R. WRIGHT, M. ZERKLE, G. ŽEROVNIK, and Y. ZHU, "ENDF/B-VIII.0: The 8th Major Release of the Nuclear Reaction Data Library with CIELO-project Cross Sections, New Standards and Thermal Scattering Data," Nuclear Data Sheets, **148**, 1–142 (2018), special Issue on Nuclear Reaction Data.

3. T. PARISH, W. CHARLTON, N. SHINOHARA, M. ANDOH, M. BRADY, and S. RAMAN, "Status of six-group delayed neutron data and relationships between delayed neutron parameters from the macroscopic and microscopic approaches," Nuclear science and engineering, **131**, 2, 208–221 (1999).
4. M. CHADWICK, P. OBLOŽINSKÝ, M. HERMAN, N. GREENE, R. MCKNIGHT, D. SMITH, P. YOUNG, R. MACFARLANE, G. HALE, S. FRANKLE, A. KAHLER, T. KAWANO, R. LITTLE, D. MADLAND, P. MOLLER, R. MOSTELLER, P. PAGE, P. TALOU, H. TRELLUE, M. WHITE, W. WILSON, R. ARCILLA, C. DUNFORD, S. MUGHABGHAB, B. PRITYCHENKO, D. ROCHMAN, A. SONZOGNI, C. LUBITZ, T. TRUMBULL, J. WEINMAN, D. BROWN, D. CULLEN, D. HEINRICHS, D. MCNABB, H. DERRIEN, M. DUNN, N. LARSON, L. LEAL, A. CARLSON, R. BLOCK, J. BRIGGS, E. CHENG, H. HURIA, M. ZERKLE, K. KOZIER, A. COURCELLE, V. PRONYAEV, and S. VAN DER MARCK, "ENDF/B-VII.0: Next Generation Evaluated Nuclear Data Library for Nuclear Science and Technology," Nuclear Data Sheets, **107**, 12, 2931–3060 (2006), evaluated Nuclear Data File ENDF/B-VII.0.
5. M. C. BRADY, Evaluation and application of delayed neutron precursor data, Ph.D. thesis (1988), copyright - Database copyright ProQuest LLC; ProQuest does not claim copyright in the individual underlying works; Last updated - 2022-02-26.
6. G. KEEPIN, T. WIMETT, and R. ZEIGLER, "Delayed neutrons from fissionable isotopes of uranium, plutonium and thorium," Journal of Nuclear Energy (1954), **6**, 1, IN2–21 (1957).
7. D. J. HUGHES, J. DABBS, A. CAHN, and D. HALL, "Delayed Neutrons from Fission of U^{235}," Phys. Rev., **73**, 111–124 (Jan 1948).
8. D. J. LOAIZA, G. BRUNSON, R. SANCHEZ, and K. BUTTERFIELD, "Measurements of Absolute Delayed Neutron Yield and Group Constants in the Fast Fission of 235U and 237Np," Nuclear Science and Engineering, **128**, 3, 270–277 (1998).
9. D. J. LOAIZA and F. E. HASKIN, "Dominant Delayed Neutron Precursors to Model Reactivity Predictions for Multiple Fissioning Nuclides," Nuclear Science and Engineering, **134**, 1, 22–36 (2000).
10. W. WIESELQUIST and R. A. LEFEBVRE, "SCALE 6.3.1 User Manual," Tech. Rep. ORNL/TM-SCALE-6.3.1, Oak Ridge National Laboratory (ORNL), Oak Ridge, TN (United States) (Feb. 2023).
11. R. E. PETERSON and G. A. NEWBY, "AN UNREFLECTED U-235 CRITICAL ASSEMBLY," Nuclear Science and Engineering, **1**, 112–125 (1956).
12. W. B. WILSON, R. T. PERRY, W. CHARLTON, T. PARISH, and E. SHORES, "SOURCES: a code for calculating (α, n), spontaneous fission, and delayed neutron sources and spectra," Radiation protection dosimetry, **115**, 1-4, 117–121 (2005).
13. J. K. TULI ET AL., "Evaluated nuclear structure data file," A Manual for Preparation of Data Sets-National Nuclear Data Center Brookhaven National Laboratory PO Box, **5000**, 11973–5000 (2001).
14. D. SAPHIER, D. ILBERG, S. SHALEV, and S. YIFTAH, "Evaluated Delayed Neutron Spectra and Their Importance in Reactor Calculations," Nuclear Science and Engineering, **62**, 4, 660–694 (1977).
15. M. C. BRADY and T. R. ENGLAND, "Delayed Neutron Data and Group Parameters for 43 Fissioning Systems," Nuclear Science and Engineering, **103**, 2, 129–149 (1989).
16. G. RUDSTAM, "Six-Group Representation of the Energy Spectra of Delayed Neutrons from Fission," Nuclear Science and Engineering, **80**, 2, 238–255 (1982).
17. T. R. ENGLAND, W. B. WILSON, R. E. SCHENTER, and F. M. MANN, "Aggregate Delayed Neutron Intensities and Spectra Using Augmented ENDF/B-V Precursor Data," Nuclear Science and Engineering, **85**, 2, 139–155 (1983).
18. C. TOFALLIS, "Least squares percentage regression," Journal of Modern Applied Statistical Methods (2009).
19. C. L. LAWSON and R. J. HANSON, Solving least squares problems, SIAM (1995).
20. M. I. RADAIDEH, W. A. WIESELQUIST, and T. KOZLOWSKI, "A new framework for sampling-based uncertainty quantification of the six-group reactor kinetic parameters," Annals of Nuclear Energy, **127**, 1–11 (2019).
21. R. TUTTLE, "Delayed-neutron yields in nuclear fission," in "Proc. Second Consultants Meeting on Delayed Neutron Properties," (1979), vol. 29.
22. R. KINSEY, L. STEWART, R. LABAUVE, P. YOUNG, A. HORSLEY, G. HALE, M. BATTAT, H. PERKINS, C. COWAN, C. FU, F. PEREY, D. FOSTER, B. MAGURNO, D. LARSON, M. ALLEN, M. DRAKE, C. PHILIS, A. SMITH, R. HOWERTON, F. MANN, A. PRINCE, T. BURROWS, S. MUGHABGHAB, M. DIVADEENAM, R. HOWERTON, M. BHAT, H. TAKAHASHI, B. LEONARD, K. STEWART, D. SARGIS, T. MAUNG, J. OTTER, C. DUNFORD, E. OTTEWITTE,

W. HENDERSON, J. ZWICK, E. KUJAWSKI, L. WESTON, and R. WRIGHT, "ENDF/B Summary Documentation," Tech. rep., Brookhaven National Laboratory (1979).
23. W. WILSON and T. ENGLAND, "Delayed neutron study using ENDF/B-VI basic nuclear data," Progress in Nuclear Energy, **41**, 1, 71–107 (2002).
24. T. ENGLAND and B. RIDER, "Status of fission yield evaluations," Tech. rep., Los Alamos National Laboratory (LANL), Los Alamos, NM (United States) (1983).